Design Study of an Edge Current Density Diagnostic Using New High-Performance Single-Channel Beam Emission Spectrometers at DIII-D

R. Albosta,[1, a)] B. Geiger,[1] G. McKee,[1] D. Den Hartog,[1] J. Schellpfeffer,[1] T. Gallenberger,[1] S. Stewart,[1] and R. Dux[2]

[1)]*Department of Engineering Physics, University of Wisconsin, Madison, 53706, United States of America*

[2)]*Tokamak: Edge and Divertor Physics, Max-Planck-Institute for Plasma Physics, 85748 Garching, Germany*

(Dated: 2 February 2023)

A novel Motional Stark Effect (MSE) spectroscopy system has been designed for application at the DIII-D tokamak. The system is optimized for studies of the poloidal and toroidal magnetic field in the plasma pedestal region with frame rates of up to 10 kHz. Light from an existing high-photon-throughput collection lens is analyzed using four single channel f/2.8 Czerny-Turner spectrometers that use custom made lens systems instead of mirrors. The spectrometers each have two separate outgoing legs and are operated in positive grating order, which allows for simultaneous observations of D-Alpha and D-Beta spectra. Forward modeling using FIDASIM shows a radial resolution of the system close to 0.6 cm, as well as sufficiently good spectral resolution when masking the high throughput light collection lens in the horizontal direction to avoid overly strong Doppler broadening of beam emission lines. Moreover, a detailed sensitivity study considering realistic levels of readout and photon noise shows that the poloidal and toroidal magnetic field strengths can be inferred with an uncertainty of less than 1% which will allow the inference of changes of the plasma current during transient events.

I. INTRODUCTION

Progress towards higher confinement in modern tokamak experiments is highly dependent on advancing our understanding on the formation and stability of the edge transport barrier[1]. The edge transport barrier suppresses turbulent transport and significantly contributes to the overall confinement properties generating a so-called pedestal in temperature and density profiles. However, details on the complex interplay of plasma currents, pressure and flows with Magneto Hydrodynamic Modes (MHD) and turbulence that form the pedestal is not well understood and therefore an active field of investigation. Novel computational models[2,3] are being developed with the goal of accurately simulating MHD mode structure and plasma parameter evolution during the transient events such as Edge-Localized Mode (ELM)[4] activity or the pedestal formation[5]. To verify these models through comparison with experimental data, sub-millisecond measurements with high accuracy are needed. While temperature and density measurements are sufficiently well developed[6], information on the edge-current density, which has both a stabilizing and destabilizing effect on the pedestal, is typically not available on sufficiently short timescales. The edge-current density profile can be inferred using Ampere's law and by studying gradients in the magnetic field, which requires accurate measurements of the strength and direction of the magnetic field at several radial locations within the pedestal. One way to collect this information is Motional Stark Effect (MSE) spectroscopy[7–9], which analyzes the Stark split emission of neutrals from neutral beam injection systems. The injected neutrals experience a strong $\vec{v} \times \vec{B}$ electric field and the emission can be observed with a substantial splitting of the angular momentum energy levels. While the magnitude of the splitting provides information on the magnetic field strength, the field direction can be determined using line-intensity ratios between the individual Stark split emission lines.

Here we present the design of a new four-channel MSE spectroscopy diagnostic with the aim of resolving the magnetic field strength and direction during transient events at DIII-D. First, the line-of-sight (LOS) geometry and spatial resolution of the new MSE system is discussed in section two. Then, the design and specifications of a new two leg spectrometer are presented in section three. Section four will show results of an initial sensitivity study, followed by a summary and outlook in section five.

II. APPLICABILITY OF THE BES LOS GEOMETRY FOR MSE MEASUREMENTS OF THE PLASMA PEDESTAL

The DIII-D tokamak is equipped with a high photon throughput light collection lens that is primarily used for BES turbulence measurements[10]. As can be seen in Fig. 1, this system views the 150° neutral beam and utilizes a collection lens with a diameter of 200 mm, which provides f/3.0 when focused at the beam-pedestal intersection. The LOS defined by the lens are nearly tangential to the magnetic field lines at the intersection with the 150° neutral beam which provides a very good spatial resolution. As shown in Fig. 2, calculations using a realistic beam and LOS geometry and a single 1 mm diameter collection fiber for each of the 4 channels provide a distorted Gaussian collection volume with a Full Width Half Maximum of about ~0.6 cm. This will provide 4 radial measurements of the magnetic field within the pedestal, yielding 3 edge-current density points for comparison with pedestal simulations. The position of these points in the plasma can be modified on a shot-to-shot basis thanks to a custom made fiber
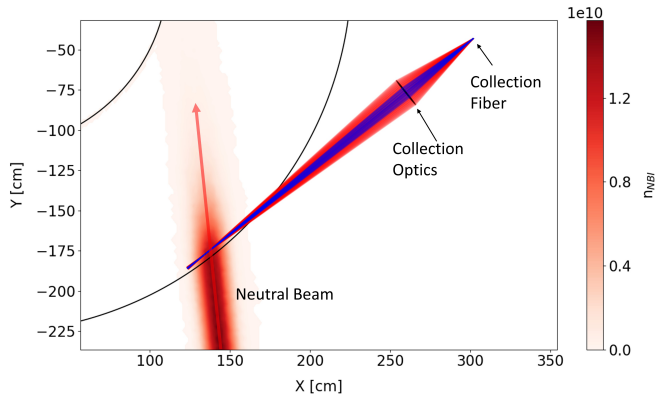
FIG. 1. Top-down view of collection lens LOS (unmasked/masked = red/blue lines) - neutral beam density [N/cm^2] (red/yellow color bar) within the outboard mid-plane pedestal at DIII-D.

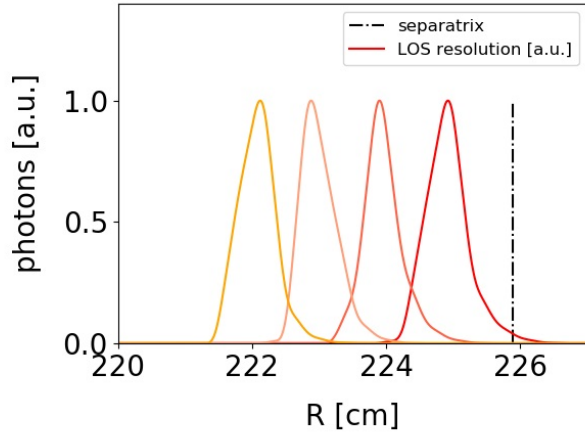holder that is mounted on a motorized stage[10].

FIG. 2. Normalized radial photon collection distribution per line of sight with 1 cm radially spaced fiber images in the plasma. The dot-dash line is the separatrix position at the outer midplane. The Full Width Half Maxima from left to right are 0.65 cm, 0.51 cm, 0.60 cm and 0.65 cm.

While the employed low F-number lens provides large photon throughput, it also covers a significant range of LOS-beam intersection angles. This leads to Doppler broadened spectra since the observed Doppler shift of the beam emission depends on these angles.

To study this Doppler Broadening effect, the code FIDASIM[11] has been employed which is capable of predicting D-alpha and D-beta spectra considering neutral beam and LOS geometries. The large lens at DIII-D has been modelled using 360 sub lines-of-sight per 1mm fiber, started at different positions on the lens as shown in Fig 3a. Considering the full lens diameter (20 cm), the D-alpha and D-beta emission spectra shown in Fig. 3b and 3c are clearly blurred and the individual Stark-split peaks can hardly be resolved. Note that the synthetic spectra consider Stark splitting, as well as the
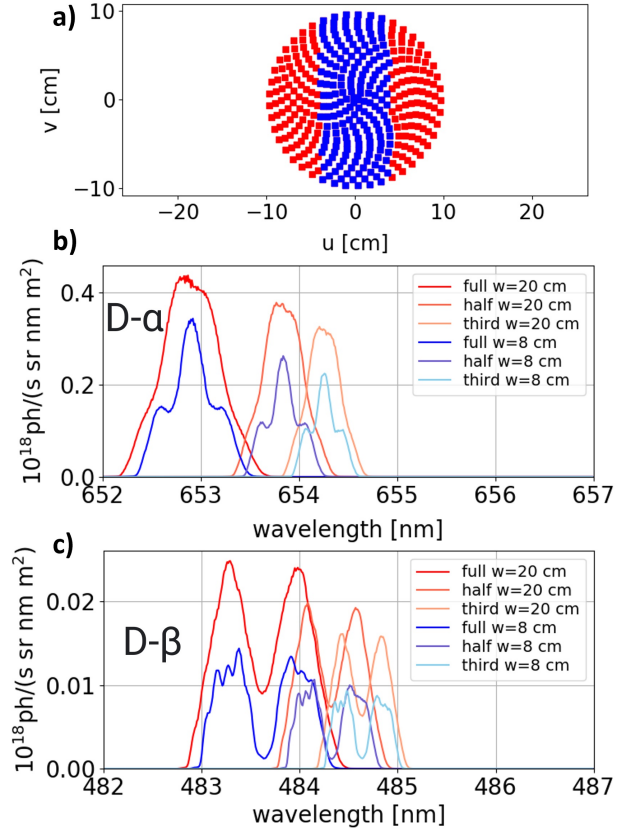

FIG. 3. **a)** Shown is the collection lens, with color-coded regions representing two lens masking options: unmasked (includes red and blue portions) and masked (only includes blue portion). **b)** D-Alpha spectrum as seen by 2 given lens masking options with 80 keV beam energy. **c)** D-Beta spectrum with same conditions

three energy components of positive neutral beams, appearing at the full, 1/2 and 1/3 of the injection energy and hence at different total Doppler shifts. When instead the horizontal width of the lens is restricted to 8 cm (throughput ≈ 55%) as shown in blue in Fig. 3, the finer Stark split structure of each energy component becomes apparent. Note here that only the left and right sides must be masked, since those correspond to changes in angle towards and away from the beam velocity direction and have a much stronger first order effect on the Doppler shift than the top/bottom of the lens. Further masking yields diminishing returns on peak quality while yielding substantially less light (2 cm width yields ≈ 15% throughput).

III. SPECTROMETER DESIGN AND SPECIFICATIONS

A novel custom made spectrometer has been designed with the aim to maximize photon throughput, while maintaining good spectral and spatial resolution. Moreover, the spectrometer design considers the capability of measuring D-alpha ($n = 3 \rightarrow 2$) and D-beta ($n = 4 \rightarrow 2$) spectra simultaneously which appear near 656 nm and 486 nm, respectively. D-alpha light is approximately two orders of magnitude brighter than the D-beta light, but the motional Stark effect is much
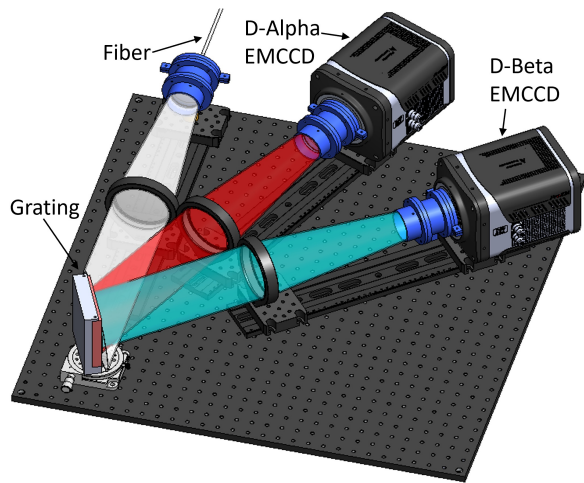
FIG. 4. 3D model of spectrometer layout. Light enters the system at an f-number of 3 through a vertical stack of 19x200 μm diameter fibers, is collimated by the first optics, diffracts off of a 2400 lines/mm grating, and enters two identical optical paths color-coded in the model for the Doppler-shifted D-Alpha and D-Beta spectra.

stronger for D-beta due to larger Stark splitting of n=4 quantum levels, compared to n=3 splitting (see e.g. Fig. 3b and 3c), yielding significantly stronger relative line splitting which improves the fitting process. Fitting both spectra simultaneously for the same plasma location allows for multi-measurement noise reduction, which lowers our noise floor significantly and allows for systematic error correction and comparison.

When aiming for measurements with high acquisition speeds, the primary limitation is the inherent photon noise (Poisson noise) present in any spectroscopic measurement. The corresponding Signal-to-Noise Ratio (SNR) scales with $\sqrt{N}$, with N being the number of photons viewed per frame.

To obtain high photon throughput, and hence high SNR, we have designed a custom made Czerny-Turner type spectrometer. This new spectrometer design makes use of a round-to-linear fiber bundle instead of an input slit, a custom-designed aspheric optical lens system with a size-matched reflecting-diffracting grating, and a modern EM-CCD detector. An overview plot of the spectrometer is shown in Fig 4.

To create the "slit", the 1mm collection fiber is coupled to a 19x200μm diameter fiber bundle, arranged in a close-packed hexagonal grid on the input side and a vertical stack on the spectrometer side. This improves on a traditional slit's light throughput by a factor of 3, with the additional height being allowable by choosing a single-channel spectrometer approach. Note that the chosen fibers are not polarization-conserving, so that the device does not need to be calibrated for polarization.

The light emitted by the round to linear fiber bundle is collimated by a lens system made of three anti-reflection coated lenses, one of which is a custom-ground asphere (manufactured by Knight Optical) designed to minimize optical aberra-
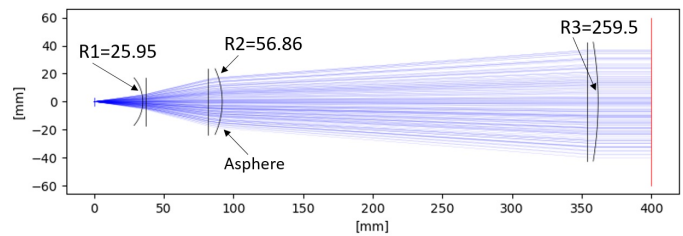

FIG. 5. Top-down view of one spectrometer optical leg. Ex: A fiber located at x=0 being collimated, to be incident on the grating.

tions while maintaining an overall focal length of 280 mm and an f-number of 2.8. Fig. 5 displays ray-tracing results for the lens system which achieves less than 30 μm spot sizes across the focal plane while maintaining high optical throughput and f-number matching with the collection optics. Detailed lens specifications are provided in figure 5.

The collimated light is then dispersed by a 102x102 mm^2 sized 2400 l/mm holographic grating from Newport, which captures the majority of the light and provides high dispersion. The grating's overall efficiency is $\sim$60% after combining both polarization state efficiencies. The grating is supported by a custom made grating holder that can be rotated using an off-the-shelf manual rotational stage. After the grating, the dispersed light is captured and focused by two additional lens systems which are identical to the one used at the spectrometer entrance. The two lenses are positioned at angles of 24 and 50 degrees relative to the incoming light and therefore allow simultaneous measurements at 656 nm and 486 nm (respectively). At the end of each lens system, a Princeton Instruments EM-CCD camera is placed, which offers low readout noise, combined with high quantum efficiency (90+%). The cameras have 512x512 square pixels with a size of 16 μm and can be operated in the so-called "fast kinetic frame transfer mode". This readout mode explored previously in[12,13], involves capturing an image in the photosensitive area (we only use the bottom 250 rows to increase speed), then the vertical binning of the image into a single row of pixels, and finally the storage of that row in the lower attached non-photosensitive CCD. The frame-rate is only limited by the shift rate of 0.45 μs/row, which translates to roughly 10 kHz for 250 vertical rows. Once 500 image rows are stored in the covered area, capture is paused and the image rows are sequentially read out. At maximum speed this produces 50 ms of capture and then 20 ms of readout, which can be repeated on this duty cycle.

Considering the specifications of the lenses, grating, opening angle, amount of pixels and pixel size, the spectrometer will have an observed wavelength range of 11.8 nm at the D-beta wavelength and 9.1 nm at D-alpha. This will be sufficient to observe not only the beam emission, but also additional spectral components such as the emission of thermal neutrals along the NBI path (also called halo) and the fast-ion D-alpha (FIDA) emission[14]. Moreover, the spectral resolution is (D-Alpha / D-Beta) 0.018 / 0.023 nm per pixel or 1.1 / 1.45 nm per mm, which is more than enough to resolve the
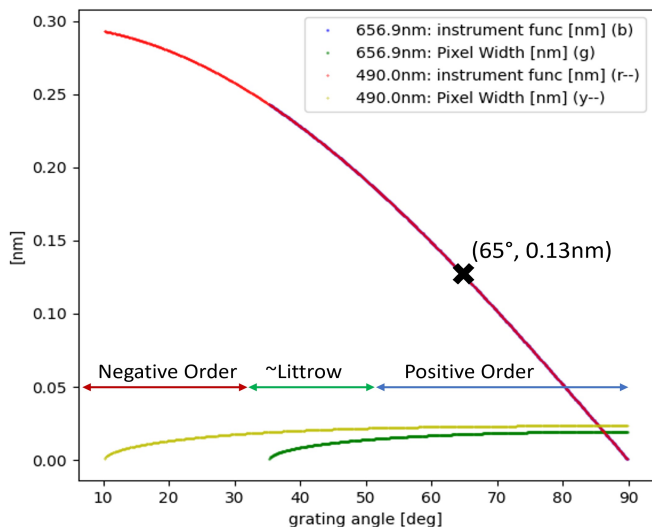
FIG. 6. Instrument function as a function of grating angle for D-Alpha (violet) and D-Beta (red) light. We have fixed the grating angle at ~ 65 degrees, which is shown as an X. At the bottom of the figure in yellow and green are the D-Beta and D-Alpha (respectively) pixel widths in nm, for reference.

beam emission. However, it should be noted that the resolving power of the spectrometer is limited by the instrumental function. The instrumental function is mainly caused by the finite size of the $200\,\mu m$ fibers at the spectrometer entrance and depends strongly on the opening angle of the spectrometer. Figure 6 shows the (rectangular-slit approximation) instrumental function as a function of the opening angle for positive and negative orders of spectrometer operation. As can be seen, operating the spectrometer in positive orders, as considered here, provides a reduced instrumental function of 0.13 nm at both wavelengths, which is acceptable as the spectral shape will be also limited by the Doppler broadening effect, which is of similar magnitude for a horizontal lens width of 8 cm. Moreover, operation in the positive order is what allows for measurements of the FIDA and halo emission, in addition to the beam emission, as this increases the spectral range. Note here, that operation in the positive order may reduce the photon throughput of a given spectrometer since the angle of incidence on the grating is larger compared to negative order. Hence, rays might miss the grating. Geometry calculations for this setup show that the photon throughput is reduced by 25% which is acceptable considering benefits from the reduced instrumental function and wider spectral range.

IV. EXPECTED PERFORMANCE

The sensitivity of the new MSE system has been assessed based on synthetic D-alpha and D-beta spectra from FIDASIM considering DIII-D discharge #179854, which is a Deuterium H-mode experiment with a core density of $6 \times 10^{19} m^{-3}$ and about 5 MW of NBI heating power. The spectra shown in figure 7 consider the masked collection lens (diameter of 8 cm in the horizontal plane), the spectrometer performance (spectral range and dispersion) and have been convoluted with the expected instrumental function, including op-

tical aberrations. Photon and readout noise have been added to the synthetic spectra to obtain realistic conditions. While the readout noise of the employed CCD camera is taken from the data sheet (3 photoelectrons), the photon noise has been determined by the Poisson law and estimating the amount of photons arriving at a given pixel of the camera per readout time. The number of photons arriving at the CCD has been calculated considering the radiance in the plasma, the etendue of the light collection optics ($0.27\,\mathrm{mm}^2$ sr), losses due to the proposed mask at the lens, the 48 m silica transmission fibers, the round-to-linear fiber bundle, the efficiency of the grating and lenses, as well as the CCD's quantum efficiency. A total amount of 7.7 nW of line-emission power is expected to arrive at the CCD for the D-alpha emission and 0.68 nW for the D-beta emission. Fig 7 shows the corresponding D-alpha and D-beta spectra with the various effects taken into account.

These spectra have then been fitted simultaneously with a forward model that has been developed for the routine analysis of spectra at DIII-D. Care has been taken to consider the skewness of individual Stark lines, caused by geometry effects[15]. A lookup table of modified gaussian parameters has been generated through sequential FIDASIM runs at different magnetic field strengths and directions which can be used to account for the non-gaussian emission line shape.

In total 17 free parameters are considered to model the D-alpha and D-beta spectra at the same time, 6 of which are fit separately to model the neutral beam halo emission. Two of these parameters are the toroidal and poloidal magnetic field strength at the intersection position between the neutral beam path and a given line of sight. A least-squares fit is used on a frame-by-frame basis, which successfully reproduces the expected line-shapes as shown in figure 7. As can be seen, the full energy component in black, half energy component in blue, and third energy component in green are well fit by the forward modeled spectra in dashed-black. As the halo emission is overlapping the beam emission, this spectral component has been included in the fit and is shown in light blue, with the total fitted spectrum plus noise in red. Bayesian analysis using the Markov Chain Monte Carlo technique within the Python package "emcee"[16] has been employed on select frames to produce error estimates and parameter weights, as shown in Fig. 8. This figure is generated from random-walk chains of the free variables, and is used to determine cross-correlation distributions between pairs of variables in the off-diagonal squares, and in the diagonals is shown the individual variable statistical distributions with the average and error bars listed above. These plots include effects from all free variables in the model, despite only 3 variables being shown. Both the FIDASIM-predicted Balmer Alpha emission and Balmer Beta emission are very well matched by the forward model, and when analyzed suggest that the poloidal and toroidal magnetic field is well constrained within 1 mT. This will allow for studies of the current density profile with a frame rate of 10 kHz and a sensitivity of about $100\,\mathrm{kA/m}^2$ at a 1 cm in-plasma spacing, with reduced uncertainty possible using wider spacing or reduced readout speeds.
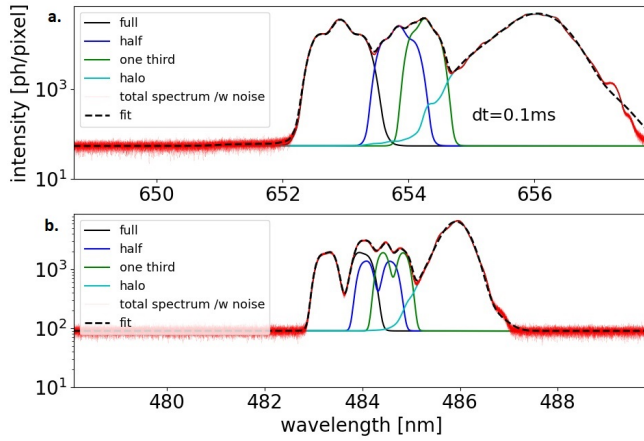
FIG. 7. Example of the advanced line profile fitting method used on a D-Alpha (**a.**) and a D-Beta (**b.**) spectrum simultaneously. The red line is the synthetic data with simulated photon and readout noise, while the black dotted line is the fit. The remaining lines display the individual components of each spectrum. The plasma edge light is eliminated by a blocking bar and not included here.
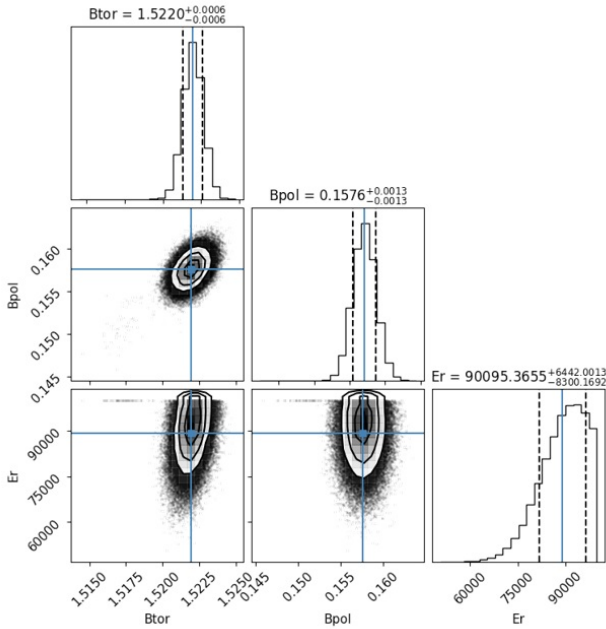

FIG. 8. Bayesian analysis results of a D-Alpha-only forward modeling run. Parameter uncertainties can be inferred by integrating the Markov Chain Monte Carlo results, as shown in the diagonal plots. The non-diagonal plots show the correlation scatter-plots between each pair of fit variables. Note that only B-poloidal [T], B-toroidal [T], and the Electric field [V/m] are shown here, but all fit variables are utilized in the analysis.

V. SUMMARY

A new high speed MSE spectroscopy system has been designed for the DIII-D tokamak which makes use of the light collection system of an existing beam emission spectroscopy system. Four single channel spectrometers are considered that use custom made lenses and are operated in the positive order of refraction which provides a reduced instrumental function and enlarged spectral range compared to the negative order.

Each of the spectrometers is equipped with two CCD cameras to simultaneously observe the Balmer alpha and Balmer beta emission. While the analysis of the Balmer alpha emission benefits from high emissivity, the Balmer beta emission provides valuable information thanks to a strong Stark splitting that is well observable even in the presence of Doppler broadening or wide instrumental functions. An initial sensitivity study suggests that the system will be capable of resolving magnetic field strengths of below 1 mT when operated with a frame rate of 10 kHz. This will allow for the study of the changes of the magnetic equilibrium during ELM crashes and pedestal formation.

VII. BIBLIOGRAPHY

[1] F. Wagner et al, Phys. Rev. Lett. **49**, 1408 (1982).

[2] G. Huysmans and O. Czarny, Nuclear Fusion **47**, 659 (2007).

[3] X. Xu, B. Dudson, P. Snyder, M. Umansky, H. Wilson, and T. Casper, Nuclear Fusion **51**, 103040 (2011).

[4] H. Zohm, Plasma Physics and Controlled Fusion **38**, 105 (1996).

[5] A. Cathey, M. Hoelzl, K. Lackner, G. Huijsmans, M. Dunne, E. Wolfrum, S. Pamela, F. Orain, and S. Günter, Nuclear Fusion **60**, 124007 (2020).

[6] M. Cavedon, R. Dux, T. Pütterich, E. Viezzer, E. Wolfrum, M. Dunne, E. Fable, R. Fischer, G. Harrer, F. Laggner, A. Mink, U. Plank, U. Stroth, M. Willensdorfer, and A. Upgrade Team, Nuclear Materials and Energy **18**, 275 (2019).

[7] N. A. Pablant, K. H. Burrell, R. J. Groebner, D. H. Kaplan, and C. T. Holcomb, Review of Scientific Instruments **79**, 10F517 (2008).

[8] R. Reimer, A. Dinklage, R. Wolf, M. Dunne, B. Geiger, J. Hobirk, M. Reich, and P. J. M. C. and, Nuclear Fusion **57**, 046005 (2017).

[9] K. H. Burrell, L. L. Lao, and B. A. Grierson, Review of Scientific Instruments **89**, 10D111 (2018).

[10] G. McKee, R. Ashley, R. Durst, R. Fonck, M. Jakubowski, K. Tritz, K. Burrell, C. Greenfield, and J. Robinson, Review of Scientific Instruments **70**, 913 (1999).

[11] B. Geiger, L. Stagner, W. Heidbrink, R. Dux, R. Fischer, Y. Fujiwara, A. Garcia, A. S. Jacobsen, A. J. van Vuuren, A. N. Karpushov, D. Liu, P. A. Schneider, I. Sfiligoi, P. Z. Poloskei, and M. Weiland, Plasma Physics and Controlled Fusion **62**, 105008 (2020).

[12] M. Cavedon, T. Pütterich, E. Viezzer, R. Dux, B. Geiger, R. M. McDermott, H. Meyer, and U. Stroth, Review of Scientific Instruments **88**, 043103 (2017).

[13] A. Jansen van Vuuren, B. Geiger, A. S. Jacobsen, M. Cavedon, R. Dux, and H. Köhnlein, Review of Scientific Instruments **90**, 103501 (2019).

[14] W. W. Heidbrink, K. H. Burrell, Y. Luo, N. A. Pablant, and E. Ruskov, Plasma Physics and Controlled Fusion **46**, 1855 (2004).

[15] R. Dux, B. Geiger, R. M. McDermott, and E. Viezzer, EPS **42**, P1.121 (2015).

[16] D. Foreman-Mackey, D. W. Hogg, D. Lang, and J. Goodman, **125**, 306 (2013), arXiv:1202.3665 [astro-ph.IM].